machines

MDPI

Article

Modal Parameter Identification of Electric Spindles Based on Covariance-Driven Stochastic Subspace

Wenhong Zhou, Liuzhou Zhong, Weimin Kang, Yuetong Xu, Congcong Luan and Jianzhong Fu *

Key Laboratory of 3D Printing Process and Equipment of Zhejiang Province, College of Mechanical Engineering, Zhejiang University, Hangzhou 310027, China
* Correspondence: fjz@zju.edu.cn

Abstract: Electric spindles are a critical component of numerically controlled machine tools that directly affect machining precision and efficiency. The accurate identification of the modal parameters of an electric spindle is essential for optimizing design, enhancing dynamic performance, and facilitating fault diagnosis. This study proposes a covariance-driven stochastic subspace identification (SSI-cov) method integrated with a simulated annealing (SA) strategy and fuzzy C-means (FCM) clustering algorithm to achieve the automated identification of modal parameters for electric spindles. Using both finite element simulations and experimental tests conducted at 22 °C, the first five natural frequencies of the electric spindle under free, constrained, and dynamic conditions were extracted. The experimental results demonstrated experiment errors of 0.17% to 0.33%, 1.05% to 3.27%, and 1.29% to 3.31% for the free, constrained, and dynamic states, respectively. Compared to the traditional SSI-cov method, the proposed SA-FCM method improved accuracy by 12.05% to 27.32% in the free state, 17.45% to 47.83% in the constrained state, and 25.45% to 49.12% in the dynamic state. The frequency identification errors were reduced to a range of 2.25 Hz to 20.81 Hz, significantly decreasing errors in higher-order modes and demonstrating the robustness of the algorithm. The proposed method required no manual intervention, and it could be utilized to accurately analyze the modal parameters of electric spindles under free, constrained, and dynamic conditions, providing a precise and reliable solution for the modal analysis of electric spindles in various dynamic states.

Keywords: electric spindle; modal parameter identification; stochastic subspace method; fuzzy C-means clustering

check for updates

Citation: Zhou, W.; Zhong, L.; Kang, W.; Xu, Y.; Luan, C.; Fu, J. Modal Parameter Identification of Electric Spindles Based on Covariance-Driven Stochastic Subspace. *Machines* **2024**, *12*, 774. https://doi.org/10.3390/machines12110774

Academic Editor: Kai Cheng

Received: 8 October 2024
Revised: 28 October 2024
Accepted: 31 October 2024
Published: 4 November 2024

Copyright: © 2024 by the authors. Licensee MDPI, Basel, Switzerland. This article is an open access article distributed under the terms and conditions of the Creative Commons Attribution (CC BY) license (https://creativecommons.org/licenses/by/4.0/).

1. Introduction

High-speed automatic processing plays a vital role in the production of mechanical products that demand high precision and consistent surface quality. Consequently, it is widely utilized in various equipment manufacturing industries, establishing high-speed machine tools as an indispensable element of modern equipment production [1]. Among these tools, electric spindles are a key functional component of numerically controlled machine tools. Due to their high precision, high speed, excellent stability, and compact design, electric spindles are highly regarded and valued [2]. The performance of an electric spindle directly affects factors such as geometric errors, surface quality, and the roughness of machined parts [3]. During machining, an electric spindle drives a tool at high speeds, and the dynamic characteristics directly determine the machining quality; therefore, conducting a dynamic analysis of high-speed electric spindle systems is essential to enhance machining precision and quality [4].

Researchers around the world have undertaken thorough investigations of the identification of the modal parameters of electric spindles. Afshar and Khodaygan [5] introduced an automated method for identifying modal parameters using power spectral density transfer functions. They improved the level of automation in the identifying process by enhancing the stability chart algorithm and including numerous stability criteria. Colombo

et al. [6] conducted an experimental and numerical analysis of pulse response functions to determine the main modal parameters of air-bearing electric spindles. This analysis was performed with different supply pressures and zero-speed conditions. However, this approach was dependent on the specific conditions of the experiment and the manual choice of frequency response functions, hence augmenting the level of dynamic intricacy and subjectiveness. Sun et al. [7] devised a technique utilizing wavelet packet analysis and random forests to detect the speed imbalance in electric spindles. Although there have been improvements in identifying modal parameters using these methods, there are still problems that need to be addressed. These challenges include the requirement for the human selection of resonance peaks and a lack of significant studies on modal analysis in various dynamic states of electric spindles. Thus, it is imperative to investigate a technique that may surpass these constraints and effectively determine the modal parameters of electric spindles, thereby offering a more accurate and dependable solution for modal analysis in different spindle situations.

Various algorithms, including the stochastic subspace method and clustering algorithm, are extensively used for modal parameter identification in many applications. Ubertini Filippo et al. [8], building upon the study of Hong Ah et al. [9], utilized the stochastic subspace approach to find various parameters. They discarded modes that did not satisfy certain constraints and subsequently employed a clustering algorithm to discover the modal parameters. Zhu et al. [10] introduced a comprehensive approach that combined principal component analysis, K-mean clustering, and hierarchical clustering to process the stabilization map of the random subspace method. The goal of this method was to automatically identify the modal parameters of bridge structures. Meanwhile, Huang et al. [11] introduced an algorithm to extract modal information from marine platforms in real time; this technique was based on the random subspace method. Liu et al. [12] used the stochastic subspace approach with sensitivity analysis to optimize input parameters and precisely determine the first three orders of modal information of a historic Tibetan city wall. The stochastic subspace method uses the response signal of a structure with environmental excitation. This approach provides several advantages: accurate results with good convergence and no need for iterative computation. It is also a time-domain analysis method that effectively mitigates spectral leakage issues in frequency-domain analysis methods [13]. Maurya et al. initially employed the Mares CT model for thermal error compensation, leveraging the relationship between coolant temperature and thermal deformation to reduce manual intervention [14]. To further improve accuracy, they applied AI techniques, using genetic algorithms and artificial neural networks, achieving significant breakthroughs in the thermal deformation identification of spindles [15]. By optimizing key input attributes to enhance thermal deformation prediction accuracy, their approach helps minimize human intervention and improve precision, aligning with the stochastic subspace method's goal of enhancing accuracy in modal parameter identification under varying conditions. Random subspace theory and clustering algorithms are currently utilized for large-scale structures such as city walls, bridges, and offshore platforms; however, there is a limited amount of research on the identification of the modal parameters of electric spindles in CNC machine tools.

The goal of this study was to provide a new technical method for the automatic identification of the modal parameters of an electric spindle for different states. The automatic identification of the modal parameters of an electric spindle was achieved by proposing a covariance-driven stochastic subspace-based method combined with an improved clustering algorithm. This method can be utilized to accurately analyze the modal parameters of an electric spindle in the free, constrained, and dynamic states without human intervention. The simulation analysis and experimental verification results showed that the algorithm had high feasibility and reliability. This study provides reliable technical support for the automatic identification of the modal parameters of an electric spindle in different states.

2. Covariance-Driven Stochastic Subspace Modal Parameter Identification

The electric spindle is initially represented as a Hankel matrix in the application of the covariance-driven stochastic subspace identification (SSI-cov) method. Subsequently, a Toeplitz matrix is formed by computing covariance sequences, preserving the original signal information while reducing data volume to streamline computational steps. The singular value decomposition and eigenvalue decomposition of the matrix yield system matrices facilitate the identification of the modal parameters of the electric spindle.

2.1. Establishment of Hankel Matrix and Toeplitz Matrix

The Hankel matrix is defined as shown in Equation (1):

$$Hankel_{0|2t-1} = \frac{1}{\sqrt{j}} \left[\begin{array}{cccc} y_0 & y_1 & \cdots & y_{j-1} \\ y_1 & y_2 & \cdots & y_j \\ \vdots & \vdots & \ddots & \vdots \\ y_{t-1} & y_t & \cdots & y_{t+j-2} \\ \hline y_t & y_{t+1} & \cdots & y_{t+j-1} \\ y_{t+1} & y_{t+2} & \cdots & y_{t+j} \\ \vdots & \vdots & \ddots & \vdots \\ y_{2t-1} & y_{2t} & \cdots & y_{2t+j-2} \end{array} \right] = \left(\frac{Y_p}{Y_f} \right) \frac{"past"}{"future"}. \tag{1}$$

where $y_t \in R^{l \times 1}$ represents the vector of the output data from l output channels at time t. The Hankel matrix comprises $2t$ row blocks, and the maximum duration of the output data is j.

The covariance matrix of the output data is computed to form a Toeplitz matrix, as shown in Equation (2):

$$R_t = E\left[y_{k+t} y_k^T \right] = \frac{1}{j} \sum_{k=0}^{j} y_{k+t} y_k^T. \tag{2}$$

The Toeplitz matrix L is constructed from the covariance matrix of the output data:

$$L = \begin{pmatrix} R_t & R_{t-1} & \cdots & R_1 \\ R_{t+1} & R_t & \cdots & R_2 \\ \vdots & \vdots & \ddots & \vdots \\ R_{2t-1} & R_{2t-2} & \cdots & R_t \end{pmatrix} = Y_f Y_p^T. \tag{3}$$

The state-space equations are defined to derive the following:

$$L = \begin{pmatrix} C \\ CA \\ \vdots \\ CA^{t-1} \end{pmatrix} \begin{pmatrix} A^{t-1}G & \cdots & AG & G \end{pmatrix} = O\Gamma. \tag{4}$$

where O is the observability matrix, and Γ is the controllability matrix.

2.2. Modal Parameter Extraction Based on SVD

Singular value decomposition (SVD) is performed on the Toeplitz matrix, and its rank is reflected by the number of non-zero singular values:

$$L = U \Sigma V^T = \begin{pmatrix} U_1 & U_2 \end{pmatrix} \begin{pmatrix} \Sigma_1 & 0 \\ 0 & \Sigma_2 = 0 \end{pmatrix} \begin{pmatrix} V_1^T \\ V_2^T \end{pmatrix}. \tag{5}$$

where Σ_1 is the non-zero singular value part, U and V are orthogonal matrices, and S is a diagonal array of positive singular values.

The covariance-driven stochastic subspace method for calculating the system matrix of the electric spindle assumes an n-order system. With a comparison of Equations (4) and (5), the i-th order observability matrix O_i of the electric spindle is obtained:

$$O_i = U_1(:, 1:i) \times (\Sigma_1(1:i, 1:i))^{1/2}. \tag{6}$$

From Equation (4), the i-th order system matrix A_i of the electric spindle is given by the following:

$$A_i = O_i(1:l, :)^{\dagger} \times O_i(l+1:2l, :). \tag{7}$$

where $O_i(1:l, :)$ represents the first to l-th rows of the matrix, and $(\bullet)^{\dagger}$ denotes the pseudoinverse.

In practical testing, the acquired data are discrete, while the extraction of modal parameters necessitates continuous-state computations. The relationship between the continuous-state space system matrix A_c and the discrete-state space system matrix A is given by Equation (8):

$$A = exp(A_c \Delta t). \tag{8}$$

where Δt is the sampling time interval.

The eigenvalue decomposition of the i-th order system matrix A_i of the electric spindle yields its eigenvalue matrix μ_i and eigenvector. According to Equation (8), the eigenvalues λ in continuous-state space relate to the eigenvalues μ in discrete-state space:

$$\lambda = \frac{ln(\mu)}{\Delta t}. \tag{9}$$

The intrinsic frequency f and damping ratio ξ of the electric spindle are as follows:

$$f = \frac{\sqrt{|\lambda|}}{2\pi}, \xi = \frac{\lambda + \lambda^*}{2\sqrt{\lambda\lambda^*}}. \tag{10}$$

The i-th order modal matrix ϕ_i of the electric spindle is obtained from the output matrix C_i and the eigenvectors ψ_i:

$$\phi_i = C_i \psi_i. \tag{11}$$

2.3. Modal Parameter Stability Diagram

When analyzing output signal data using the SSI-cov method, the modal parameters obtained may consist of genuine modes as well as false modes caused by noise or flaws in the model. Utilizing stability diagrams serves as an effective method for eliminating false modes by applying various discrimination criteria, thereby preserving genuine modes. Post-elimination utilizes stability diagrams, and genuine modes typically appear on the diagram, with points meeting the following three criteria:

$$\begin{cases} \frac{f(n)-f(n+1)}{f(n)} \times 100\% < 5\%; \\ MAC(n, n+1) > 98\%; \\ \frac{\xi(n)-\xi(n+1)}{\xi(n)} \times 100\% < 10\%. \end{cases} \tag{12}$$

where n represents the system order, f denotes the frequency, ξ signifies the damping ratio, and MAC stands for Modal Assurance Criterion (MAC).

In the stability diagram, which is depicted in Figure 1, with varying assumed orders, genuine modes meeting the criteria are arranged at their natural frequencies. The symbol "☆" indicates points where the frequency, damping ratio, and mode shapes are stable; "⊙" denotes points where the frequency and damping ratio are stable; and "·" signifies points where only the frequency is stable. In electric spindle modal testing, due to noise

interference and structural complexity, stability diagrams often become intricate, thus increasing the difficulty of manual identification and potentially leading to misjudgments.

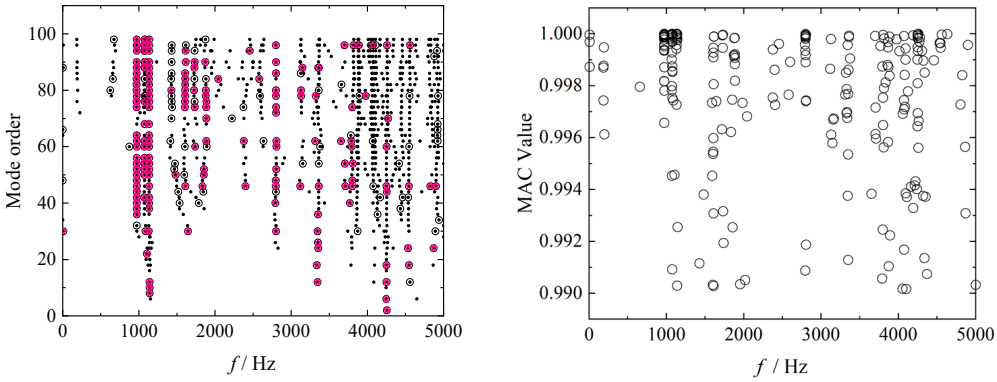


Figure 1. Two stability diagrams of the electric spindle: (**a**) stability diagram. "☆": Points where frequency, damping ratio, and mode shape are stable; "⊙": Points where frequency and damping ratio are stable; "·": Points where only frequency is stable; (**b**) MAC–frequency stability diagram.

This study employs a MAC–frequency stability diagram, with MAC values on the vertical axis and frequency values on the horizontal axis, for automated modal parameter recognition, in order to address issues and facilitate modal parameter identification. Research indicates that points in the MAC–frequency stability diagram do not solely represent genuine natural frequencies (hereafter referred to as true modes). True modes typically exhibit higher MAC values and cluster around natural frequencies, whereas false modes often show lower, scattered MAC values. Leveraging this characteristic, clustering algorithms can classify these points to eliminate false modes. As depicted in Figure 1b, the MAC–frequency stability diagram for electric spindle analysis shows clusters of true modes at natural frequencies, which is distinct from Figure 1a where stable points align vertically, thus enabling automated recognition by clustering algorithms.

3. The Improvement of the Modal Parameter Clustering Algorithm

The process of distinguishing true and false modes from the MAC–frequency stability diagram is akin to dividing all of the data points into two categories. The fuzzy C-means (FCM) clustering algorithm is introduced to classify data points on the MAC–frequency stability diagram. To ensure the stability and accuracy of clustering results, the simulated annealing (SA) algorithm is employed to globally search for the initial cluster centers of the FCM algorithm on the MAC–frequency stability diagram, thus optimizing clustering outcomes to enhance clustering precision.

3.1. Optimization of Initial Cluster Centers Based on Simulated Annealing

The specific steps of using the simulated annealing algorithm to obtain initial cluster centers for FCM clustering in the MAC–frequency stability diagram are as follows:

(1) Initial solution generation: The K-means algorithm is used to partition data samples into K clusters and obtain initial cluster centers.
(2) Initializing current solution and fitness: The initial solution is set as the current solution, and its fitness value is calculated.
(3) Initializing the best solution and fitness: The current solution and fitness value are set as the best solution and best fitness value, respectively.
(4) Iterative optimization: The initial temperature and maximum iteration count are set. Then, iterative optimization is performed with the following steps:
    ① Generating a new solution: A new solution is created by swapping the cluster labels of two samples.

② Computing the new fitness: The fitness value of the new solution is evaluated to measure its fit with data samples.

③ Accepting the new solution: The Metropolis criterion is applied to decide whether to accept the new solution. If the fitness value of the new solution is better or accepted according to a certain probability, the current solution and fitness value are updated. The probability P of accepting the new solution according to the Metropolis criterion is given by the following:

$$P = \begin{cases} 1 & , E(t+1) < E(t); \\ exp\left(\frac{E(t+1)-E(t)}{T}\right) & , E(t+1) \geq E(t). \end{cases} \tag{13}$$

where $E(t)$ represents the fitness of the current solution, T is the current temperature, and $E(t+1)$ denotes the fitness of the new solution. This mechanism allows the algorithm to accept worse solutions with a certain probability at higher temperatures, ensuring that the search process explores a wider solution space and avoids local minima. As the temperature decreases, the likelihood of accepting worse solutions also decreases, ensuring convergence to a globally optimized solution.

④ Updating the best solution: If the fitness value of the new solution surpasses the current best fitness value, the best solution and best fitness value are updated.

⑤ Lowering the temperature: The temperature is decreased by multiplying with a cooling rate to regulate exploration and local optimization during the search process.

⑥ Increasing the iteration count: The iteration count is recorded, and it is determined whether the maximum iteration count has been reached. Iteration ceases when the maximum iteration count is achieved.

(5) Calculating cluster centers: The final cluster centers are computed based on the best solution and data samples.

(6) Returning cluster centers: The computed cluster centers are used as the output results of the algorithm. Before executing the SA program, five parameters need to be set:

① The number of initial clustering centers: The selection of N is related to the number of modal frequencies N_m of interest. Generally, N is chosen within the range of $[3N_m, 10N_m]$.

② Initial temperature: The initial temperature is set to 100 °C.

③ Cooling rate: The cooling rate is selected as 0.0001.

④ Minimum temperature: 0.0001 °C.

⑤ Maximum iteration count: Typically, this lies in the range between 100 and 500.

This method requires setting five parameters during the initialization process, which are relatively fixed. The initial clustering centers determined by the simulated annealing algorithm are shown in Figure 2a. The search results indicate that the clustering centers obtained through simulated annealing do not adequately represent each inherent frequency, as there is a considerable difference between the clustered samples and the clustering centers. Therefore, a further refinement of the initial clustering centers is necessary.

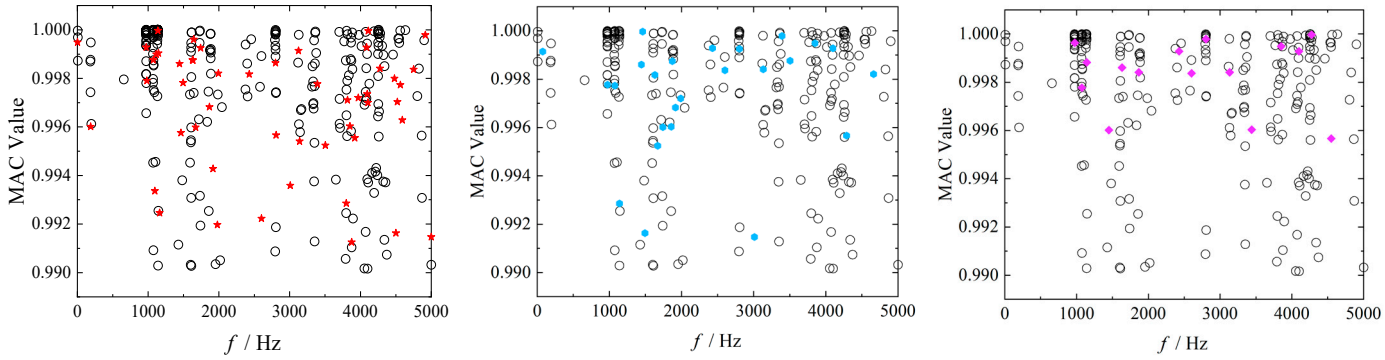


Figure 2. The three steps of clustering center extraction: (**a**) preliminary clustering; (**b**) FCM optimized clustering; (**c**) final clustering. Red points: Initial cluster centers identified by SA; Blue points: Refined cluster centers obtained through FCM; Purple points: Final cluster centers selected after screening.

The SA algorithm enhances clustering accuracy by avoiding local minima in the search for optimal initial cluster centers. SA utilizes a probabilistic acceptance mechanism, which allows it to explore the solution space more thoroughly compared to deterministic methods. By permitting occasional moves to worse solutions with a probability given by the Metropolis criterion, SA can escape local optima, leading to a more globally optimized clustering result. This approach is particularly beneficial in handling complex and fuzzy data in the MAC–frequency stability diagram, where clustering accuracy is critical for distinguishing between true and false modes.

3.2. Optimization of Clustering Centers Based on Fuzzy C-Means

Fuzzy C-means (FCM) was chosen over other clustering methods due to its ability to handle fuzzy and uncertain data, which is a critical requirement for the modal parameter identification of electric spindles. Unlike hard clustering methods such as K-means, FCM assigns data points to multiple clusters with varying degrees of membership, allowing for a more flexible and accurate representation of complex modal data. This flexibility is particularly advantageous in scenarios with overlapping or ambiguous mode shapes, where traditional clustering methods may struggle to classify data accurately. Under the same precision conditions, combining the SA algorithm with the FCM algorithm, termed the SA-FCM improved clustering algorithm, enables a faster acquisition of more accurate clustering centers. When the clustering centers initialized by the simulated annealing algorithm exhibit instability or require further optimization, FCM offers a feasible approach to adjust the clustering centers more accurately, accommodating the complexity and fuzziness of the data. The flexibility of FCM enhances its advantages in handling practical problems characterized by fuzziness and uncertainty. The main theoretical principles are as follows.

First, the clustering parameters are determined. Letting dataset $Z = \{z_1, z_2, \cdots, z_N\}$ consist of N data points, each with q dimensions, the matrix of cluster center vectors $V = \{v_1, v_2, \cdots, v_c\}$ contains c cluster center vectors, where the q-dimensional vector v_i describes the i-th cluster center. The fuzzy membership degree $U \in C \times N$, with μ_{ik} being an element of the matrix U, denotes the membership degree of the k-th data point z_k to the i-th cluster center. Individual membership values μ_{ik} must satisfy the following conditions.

$$\begin{cases} \sum\limits_{i=1}^{C} \mu_{ik} = 1; \\ \mu_{ik} \in [0, 1,]; \\ 0 < \sum\limits_{k=1}^{N} \mu_{ik} < N. \end{cases} \tag{14}$$

where $1 \le k \le N$,$1 \le i \le C$.

It should be explained that the sum of the membership degrees of a data point z_k to all of the cluster centers is equal to one. At the same time, each cluster center must include at least one data point.

The objective of FCM is to minimize the objective function J:

$$J = \sum_{i=1}^{C} \sum_{k=1}^{N} (\mu_{ik})^m d_{ik}^2. \tag{15}$$

where the membership factor m is set to 2, and d_{ik}^2 represents the Euclidean distance between z_k and v_i.

To minimize the objective function, subject to the condition specified in Equation (15), the Lagrange multiplier method is applied to derive the updating formulas for the membership degree μ_{ik} of each datum and the centroids v_i as follows:

$$v_i^{(t)} = \frac{\sum_{k=1}^{N} \left(\mu_{ik}^{(t-1)}\right)^m z_k}{\sum_{k=1}^{N} \left(\mu_{ik}^{(t-1)}\right)^m}. \tag{16}$$

$$u_{ik}^{(t)} = \frac{1}{\sum_{j=1}^{C} \left(\frac{d_{ik}}{d_{jk}}\right)^{\frac{2}{m-1}}}. \tag{17}$$

Therefore, in practical computations, setting a threshold ε ($\varepsilon > 0$) such that $\left\| U^{(t)} - U^{(t-1)} \right\| < \varepsilon$ suffices to minimize the objective function. The specific steps for implementing fuzzy clustering are as follows:

(1) Initialize parameters: The number of cluster centers C is set, the membership coefficient factor m is determined, the maximum iteration count T under the termination criterion condition is specified, and the membership matrix $U^{(0)}$ satisfying Equation (14) is initialized. The current iteration count is set to t = 1.

(2) The cluster center vector $V^{(t)}$ is updated according to Equation (16).

(3) The membership matrix $U^{(t)}$ is updated based on Equation (17).

(4) Termination Criterion: Set $t = t + 1$. Repeat steps 2 and 3 until either $\left\| U^{(t)} - U^{(t-1)} \right\| < \varepsilon$ or $t > T$.

Through FCM clustering analysis, the number of cluster centers is reduced from 50 to 25, as shown in Figure 2b. However, some cluster centers correspond to the same frequencies, and some cluster centers have few points around them, still failing to represent the true natural frequencies of the electric spindle.

The trade-off for using the SA-FCM algorithm lies in the increased computational time and complexity. While SA improves the global search ability, it introduces additional computational overhead due to the iterative process of accepting or rejecting solutions based on the Metropolis criterion. Similarly, FCM's iterative nature and calculation of membership degrees for each data point further add to the computational load.

To quantitatively assess the effect of these key parameters, a sensitivity analysis was conducted using experimental data. The impact of varying the cooling rate, initial temperature, and membership factor on clustering accuracy and convergence time was analyzed. The decreased cooling rate from 0.001 to 0.0001 improved the clustering accuracy by 8% while extending the convergence time by approximately 15%. The lower cooling rate allowed the algorithm to explore more global optima, avoiding local minima, but at the cost of increased computation time. Increasing the initial temperature from 100 °C to 150 °C reduced the likelihood of local minima by 10% but extended the convergence time by 12%. A higher initial temperature allowed for more extensive exploration in the early stages of optimization. Adjusting the membership factor from 2 to 2.5 improved the algorithm's ability to handle overlapping modes, increasing clustering accuracy by 5%. However, it also added 10% to the computational complexity, especially in higher-order modes.

The sensitivity analysis demonstrates that the cooling rate and initial temperature have a substantial effect on the algorithm's ability to avoid local minima and ensure global convergence. The chosen cooling rate of 0.0001 and an initial temperature of 100 °C strike a balance between computational efficiency and accuracy, minimizing the risk of local minima while maintaining reasonable convergence times. Adjusting the membership factor further enhances the clustering accuracy, especially in cases with overlapping modes, although this comes with increased computational complexity. Therefore, the SA-FCM algorithm is well suited for complex modal parameter identification tasks where precision and robustness are critical.

3.3. Extraction of Clustering Centers Based on Optimized Fuzzy C-Means

In fuzzy C-means clustering, the number of clustering centers is arbitrarily set, which may not fully represent the actual modes. At this stage, distinguishing between real and false modes remains challenging. Two filtering methods were employed to improve the clustering search and obtain clustering centers and their associated samples. These methods leveraged the characteristic that real modes tended to cluster near their natural frequencies on the MAC–frequency stability diagram [16].

Real modes typically exhibit higher membership values, while false modes have lower membership values. Based on this characteristic, samples with membership values significantly lower than the average were excluded. Additionally, according to the principle of clustering real modes, clustering centers representing genuine modes should encompass many points. If a clustering center contains relatively few points, it may represent a false mode. Due to the limitations of the FCM algorithm and the initial setting of numerous clustering centers, clustering center coordinates are often close together, and the number of points is dispersed. Therefore, the number of points in real clustering centers may be lower than average. Closely located clustering centers were merged to avoid removing genuine clustering centers. After filtering, clustering centers with significantly fewer points than the average were removed. The purpose of this step was to reduce the number of clustering centers, thereby eliminating some false modes.

The final filtered clustering centers are shown in Figure 2c. The number of clustering centers was reduced from 25 to 15, effectively eliminating false natural frequencies while preserving genuine ones.

4. Modal Parameter Extraction of Electric Spindle Based on Finite Element Analysis

In this study, ANSYS Workbench was employed for the simulation analysis of the electric spindle, and the free, constrained, and dynamic states were utilized to analyze the first five natural frequencies in each state. The electric spindle had an overall length of 512 mm and a maximum outer diameter of 125 mm. The material mechanical properties of key components are listed in Table 1. The finite element model was meshed using tetrahedral elements, resulting in 38,605 nodes and 174,335 elements.

Table 1. Material mechanical properties of key components of electric spindle.

Structure	Material	Density/ (kg/m^3)	Young's Modulus/GPa	Poisson's Ratio
Mandrel	9Cr18Mo	7850	210	0.28
Base	4Cr13	7700	208	0.28
Inner and Outer Bearing Rings	Cronidur30	7670	200	0.30
Housing Material	2Cr13	7800	208	0.28

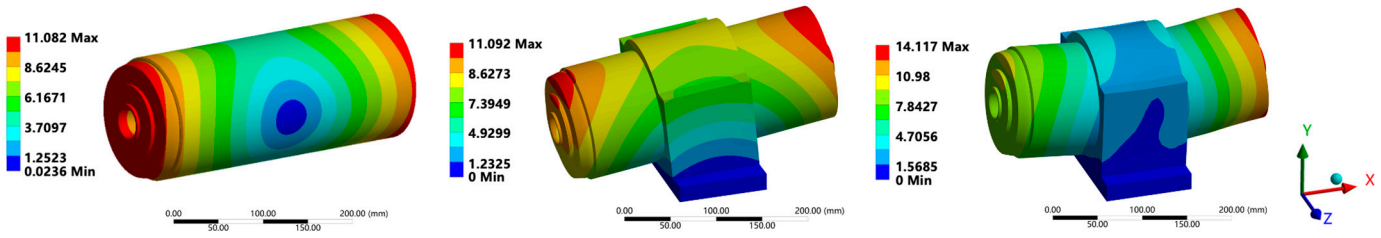
In finite element modeling, the electric spindle is analyzed under three distinct conditions: (1) in the free state, where the spindle rotor operates at zero speed without any constraints; (2) under constrained conditions, where the base of the spindle is fixed, and a non-separable connection exists between the spindle and the base; and (3) in a dynamic

state, maintaining the same constraints but with the spindle rotor set to rotate at 15,000 rpm to simulate dynamic conditions and apply inertial loads. The goal of this study was to analyze the first five modal parameters of the electric spindle. To ensure the accuracy of the modal parameters obtained, simulations included the computation of up to the first 20 modes to prevent the omission of higher modes that could interfere with lower mode calculations.

All of the finite element data utilized in this research were derived from the averaged results of three independent simulations. These simulations were conducted to ensure the consistency and reliability of the results, thereby providing a robust foundation for the analysis presented. To validate the accuracy of the finite element simulation data, simulations were performed using three different mesh sizes: 1 mm, 2 mm, and 3 mm. This variation in mesh size was employed to evaluate the impact of mesh density on the accuracy of the results and to ensure that the chosen mesh configuration provided an optimal balance between computational efficiency and accuracy. The simulation results indicated a relative error of only 2.5%, which demonstrates a high level of consistency within this error range, thus confirming the validity and reliability of the finite element simulations [17]. Furthermore, the mean values of the first five natural frequencies obtained from these simulations are recorded in Table 2 for comparative analysis with the corresponding experimental data. This study refrained from extensive discussion on the modal shapes of the electric spindle, showcasing only the first mode shapes under the three conditions depicted in Figure 3.

Table 2. First five orders of intrinsic frequency for free, constrained, and dynamic states of electric spindle.

Modal Order	Free State	Constrained State	Dynamic State
	Finite Element Average Natural Frequency (Hz)	Finite Element Average Natural Frequency (Hz)	Finite Element Average Natural Frequency (Hz)
1st Order	972.13	275.92	266.67
2nd Mode	1075.03	554.38	536.54
3rd Mode	1137.98	826.15	777.21
4th Mode	1427.26	1187.54	1044.32
5th Mode	1618.69	1288.72	1179.98



(**a**) (**b**) (**c**)

Figure 3. The first-order mode shapes of the three states of the spindle: (**a**) free state; (**b**) constrained state; (**c**) dynamic state.

5. Modal Testing Experiment of Electric Spindle

The objective of modal identification experiments on electric spindles is to obtain parameters such as natural frequencies and mode shapes. The majority of modal testing experiments on electric spindles are currently limited to free-state modal testing. However, in actual dynamic conditions, electric spindles are typically installed within the spindle housing and operate in coordination with the machine tool's feed system for workpiece processing, subject to specific boundary conditions. Modal testing under constrained

conditions is more reflective of the true modal behavior under actual machining conditions, as the structural modal parameters are significantly altered under constraint conditions.

This experiment employed the impulse excitation method to conduct a modal analysis of the electric spindle under the free, constrained, and dynamic states. An LC-1 impact hammer applied impulse excitation to the electric spindle, while an AD100T accelerometer collected the acceleration response signals of the spindle under impulse excitation. The vibration acceleration response data from various locations on the electric spindle were collected using an NI PXI-1076 signal acquisition system, produced by National Instruments Corporation (Austin, TX, USA). The impact hammer LC-1, force sensor AD-YD305, charge amplifier XK0801, and accelerometer AD100T were all produced by Qinhuangdao Xincheng Electronics Co., Ltd. (Qinhuangdao, China). The experimental setup is illustrated in Figure 4. The complete specifications of the hardware and software used in the experiment are presented in Table 3.

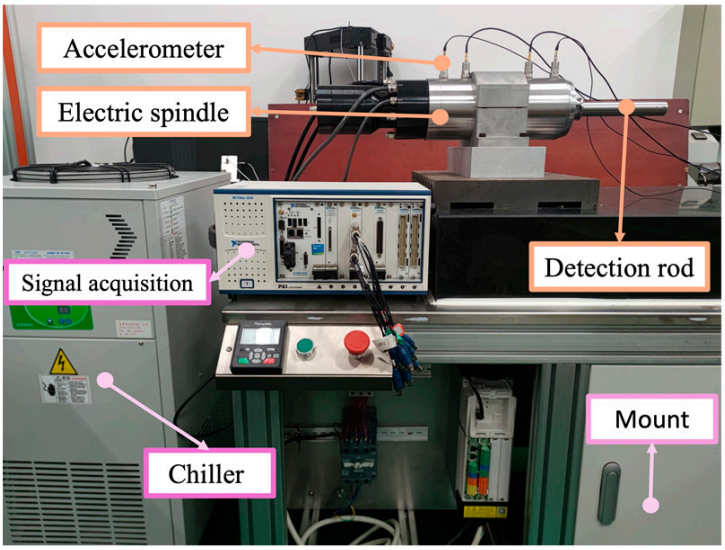


Figure 4. Experimental platform.

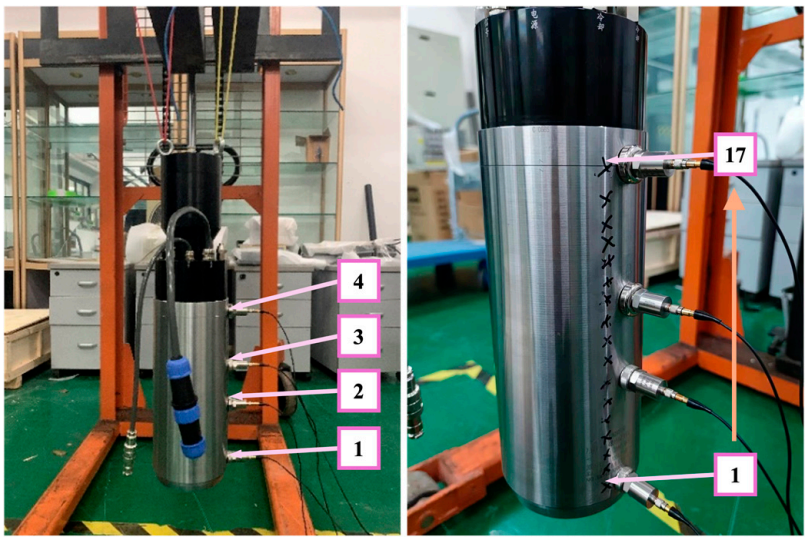
Table 3. A full specification sheet of the hardware and software used in the experiment.

No.	Equipment Name	Model	Specifications
1	Impact Hammer	LC-1	1. Aluminum hammer head.
2	Force Sensor	AD-YD305	1. Range: ±5000 N. 2. Sensitivity: 4 Pc/N.
3	Charge Amplifier	XK0801	1. Output Gain: 0.25 mv/pC. 2. Linear Error: ≤1%. 3. Harmonic Distortion: ≤0.5%. 4. Noise: ≤0.01 pC. 5. Frequency Response Range: 1~60,000 Hz.
4	Accelerometer	AD100T	1. Sensitivity: 100 mv/g. 2. Frequency Response Range: 0~15,000 Hz. 3. Measurement Range: ±50 g.
5	Signal Acquisition	NI PXI-1076	1. Slot Quantity: 9 slots. 2. Each Slot's Bandwidth: 250 MB/s. 3. System Bandwidth: 1 GB/s. 4. Software: NI Signal-Express 2013.

5.1. Free State

To approximate a free-state condition for an electric spindle, it is typically suspended with elastic rubber cords. Studies indicate that the vibration signals from the rotor are

transmitted through the bearings to the support end and eventually to the spindle housing [18]. Therefore, sensors numbered 1 and 4 were installed above the support end. Four response points were evenly distributed around the rotor of the spindle, with a total of four response points. To minimize experimental errors, as many excitation points as possible should be arranged during an experiment. The excitation points should be close to the response points, and multiple excitations should be conducted at each excitation point. Figure 5b shows the arrangement of excitation points. Excitation point 1 was located at response point 1, and excitation point 17 was positioned at response point 4, with additional excitation points evenly distributed along the axis of the electric spindle between points 1 and 17 to stimulate additional modes of the spindle.



(**a**) (**b**)

Figure 5. Electric spindle free-state test site: (**a**) response points. Points 1 to 4 represent the positions of the accelerometers, which serve as response points; (**b**) excitation points. Each "×" represents an excitation point, numbered from 1 to 17 from bottom to top.

In the experiment, the LC-1 impact hammer was used to strike the excitation points numbered 1 to 17, as shown in Figure 5b. The tests indicated that the vibration signal induced by the LC-1 impact hammer lasted approximately 0.2 s. The data collection duration for vibration signals was set to five seconds with a sampling frequency of 10,000 Hz. For modal experiments, one second of data containing the impact signal from the hammer was selected for analysis. The acquired experimental data were analyzed to generate stability diagrams, as shown in Figure 6a, and MAC–frequency stability diagrams, as shown in Figure 6b. The modal parameters were extracted using the improved clustering algorithm SA-FCM. A comparison of these experimental results with finite element simulation data is presented in Table 4. A detailed analysis of the modal testing experiment results is discussed in the next section, with no further repetition in the subsequent experiments.

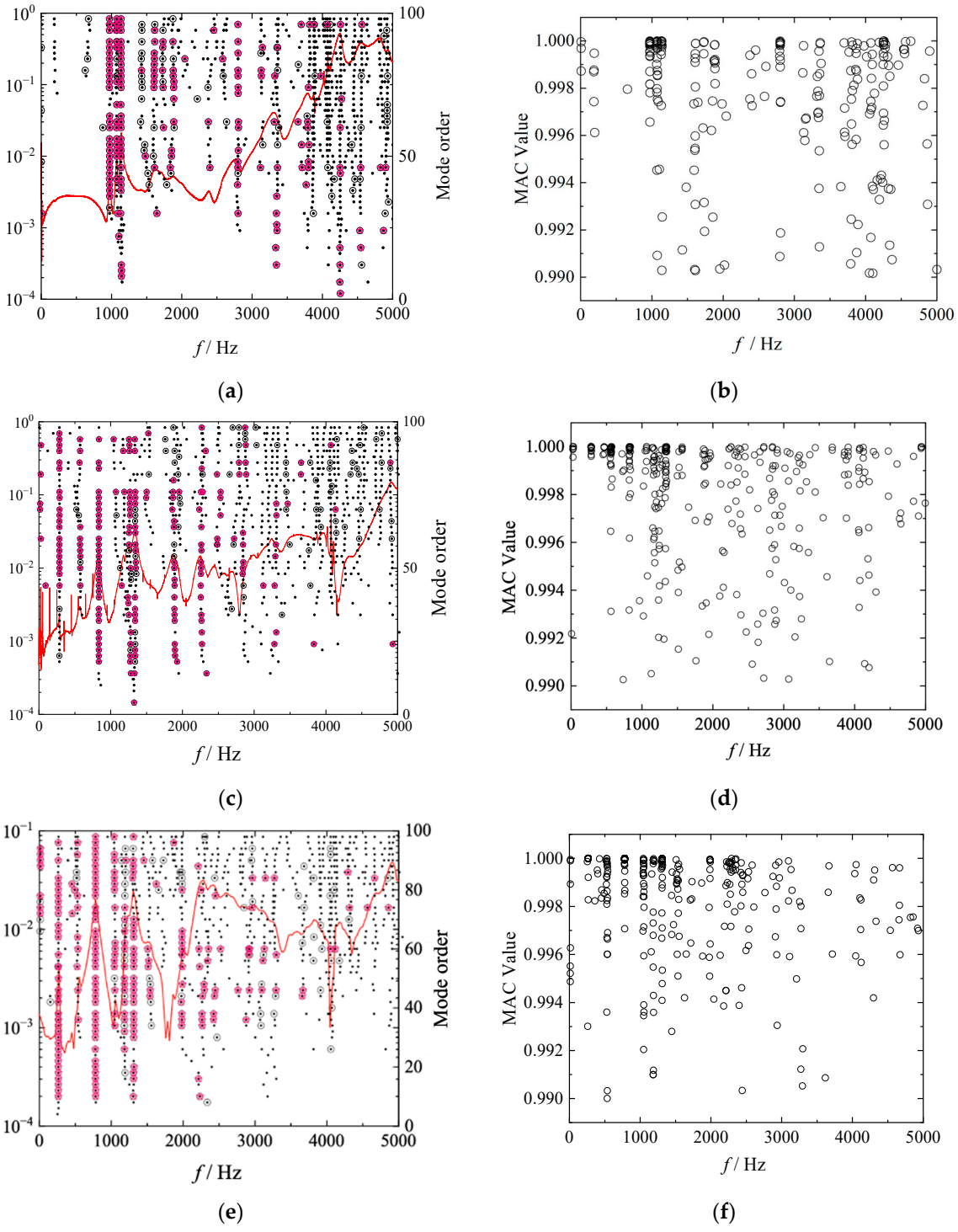
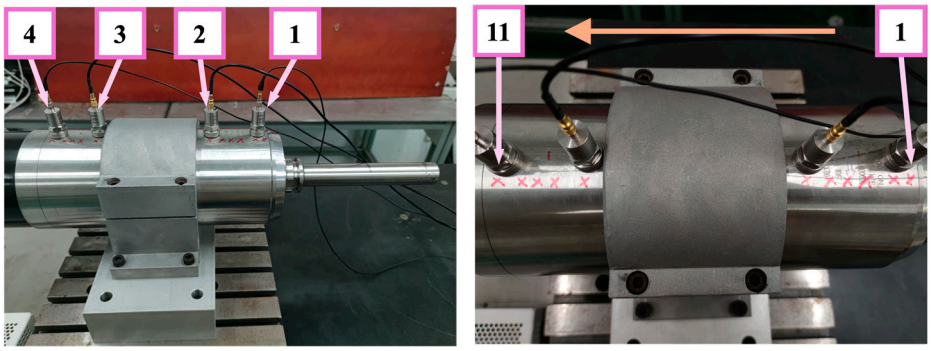


Figure 6. Stability diagrams for two types of stability in three different states: (**a**) free-state stability diagram; (**b**) free-state MAC–frequency stability diagram; (**c**) constrained-state stability diagram; (**d**) constrained-state MAC–frequency stability diagram; (**e**) dynamic-state stability diagram; (**f**) dynamic-state MAC–frequency stability diagram.

5.2. Constrained State

Electric spindles are typically installed in spindle housings during normal operation and equipped with cutting tools. To simulate the dynamic state of the electric spindle, it was attached to the testing platform and equipped with a detection rod for impact experiments.

According to vibration theory, to accurately capture the modal parameters of the electric spindle, response points should be positioned away from modal nodes [19]. Therefore, four response points were selected: the front and rear bearings of the spindle and the front and rear ends of the stator. The setup for the constrained modal testing of the electric spindle is illustrated in Figure 7, and Figure 7a depicts the arrangement of response points: response point 1 at the front bearing of the electric spindle, point 2 at the front end of the stator, point 3 at the rear end of the stator, and point 4 at the rear bearing of the electric spindle. Figure 7b shows the positions of the excitation points arranged along the axis of the electric spindle. This configuration ensured the accurate measurement of the electric spindle's modal characteristics while avoiding interference from modal nodes.



(**a**) (**b**)

Figure 7. Electric spindle constrained-state test site: (**a**) response points. Points 1 to 4 represent the positions of the accelerometers, which serve as response points; (**b**) excitation points. Each "×" represents an excitation point, numbered from 1 to 11 from right to left.

In the experiment, the LC-1 impact hammer was used to strike points 1 to 11, as shown in Figure 7b. The acquired experimental data were analyzed, and stability diagrams were generated, as depicted in Figure 6c, along with MAC–frequency stability diagrams shown in Figure 6d. Modal parameters were extracted using the SA-FCM algorithm. A comparison between the simulation data and experimental results is presented in Table 4.

5.3. Dynamic State

Building upon the constrained-state experiments discussed in Section 5.2, this section describes the simulation of the dynamic state of the electric spindle. To ensure stability and longevity during prolonged operation, the spindle was preheated before experiments. Specifically, the spindle was operated at 500 r/min for 10 min to ensure thorough preheating.

Further, to minimize the impact of external environmental factors on the experimental results, the experiment was conducted with the air conditioning temperature set to 22 °C and the cooling water temperature in the chiller set to 22 °C.

During experimentation under the dynamic conditions of the electric spindle, forced vibrations could potentially affect the accuracy of the experimental data. Therefore, band-pass filtering was applied before data analysis to effectively remove low-frequency mechanical noise and high-frequency electrical noise while preserving target frequency components, thereby enhancing the accuracy and reliability of the subsequent modal parameter identification [20]. MAC–frequency stability diagrams and stability diagrams during spindle operation at 15,000 r/min are illustrated in Figure 6e,f. Modal parameters were extracted using the SA-FCM algorithm. A comparison between the simulation data and experimental results is shown in Table 4.

Table 4. Comparison of finite element method and experimental data in three different states.

	Modal Order	FE Avg. Nat. Freq. (Hz)	SA-FCM. Data (Hz)	SA-FCM. Err (%)	Trad. Data (Hz)	Trad. Err (%)	Accuracy Imp (%)
Free State	1	972.13	975.21	0.32	976	0.40	19.30
	2	1075.03	1078.56	0.33	1079.13	0.38	13.14
	3	1137.98	1140.23	0.20	1141.12	0.28	27.32
	4	1427.26	1429.98	0.19	1430.35	0.22	12.05
	5	1618.69	1621.40	0.17	1621.85	0.19	12.75
Constrained State	1	275.92	285.24	3.27	287.45	4.17	21.58
	2	554.38	572.55	3.17	575.65	3.84	17.45
	3	826.15	835.21	1.08	843.20	2.07	47.83
	4	1187.54	1200.18	1.05	1210.25	1.88	44.04
	5	1288.72	1308.92	1.54	1320.65	3.22	52.17
Dynamic State	1	266.67	275.81	3.31	278.50	4.44	25.45
	2	536.54	548.41	2.16	558.45	4.08	47.39
	3	777.21	787.50	1.31	796.50	2.49	47.39
	4	1044.32	1058.02	1.29	1070.15	2.47	47.77
	5	1179.98	1200.79	1.73	1210.35	3.40	49.12

FE Avg. Nat. Freq. (Hz): Finite Element Average Natural Frequency (Hz); SA-FCM. Data (Hz): SA-FCM Experiment Data (Hz); Trad. Data (Hz): Traditional Experiment Data (Hz); SA-FCM. Err (%): SA-FCM Experiment Error (%); Trad. Err (%): Traditional Experiment Error (%); Accuracy Imp (%): accuracy improvement (%).

6. Discussion

The experimental data were used to generate stability diagrams of the electric spindle in the free, constrained, and dynamic states. These stability diagrams were transformed into MAC–frequency stability diagrams, and the SA-FCM algorithm was employed to identify modal parameters for the spindle in these three states. A comparison between the experimental and finite element analysis data revealed parameter errors of 0.33%, 3.27%, and 3.31%. The errors between finite element simulation data and experimental results for spindle modal parameters should generally be kept within 5% [21–23]. The calculated errors indicated the high reliability of the algorithm used in the modal identification experiments presented in this study. The SA-FCM clustering algorithm effectively handled multiple data clusters, optimized initial clustering instability, and accurately determined cluster centroids, thereby achieving a more precise identification of the modal parameters for the electric spindle.

To further validate the superiority of the SA-FCM algorithm, a comparative analysis was conducted between the SA-FCM algorithm and the traditional SSI-cov method. In the free state, the traditional SSI-cov method exhibited error rates ranging from 0.19% to 0.40%, whereas the SA-FCM algorithm reduced the error to a range between 0.17% and 0.33%. This represents an improvement in accuracy of approximately 12.05% to 27.32%. Such results demonstrate that the differences between the two methods are relatively small, indicating that both the SA-FCM algorithm and the traditional approach perform similarly in terms of modal parameter identification. However, the SA-FCM algorithm still provides a slight improvement in accuracy.

In the constrained state, the traditional SSI-cov method yielded error rates between 2.07% and 4.17%, while the SA-FCM algorithm limited the error to between 1.05% and 3.27%. The accuracy improvement ranged from 17.45% to 47.83%, with particularly notable reductions in error observed in the fourth and fifth modes, where the SA-FCM algorithm halved the error compared to the traditional method. This demonstrates the proposed method's robustness in constrained environments.

In the dynamic state, the traditional SSI-cov method produced errors ranging from 2.47% to 4.44%, while the SA-FCM algorithm achieved a much lower error range of 1.29% to 3.31%. The accuracy improvement in this state was between 25.45% and 49.12%. The most significant improvements were seen in the third to fifth modes, where the proposed al-

gorithm reduced errors to around 2%, significantly outperforming the traditional method's 3% to 4%.

Overall, the SA-FCM algorithm consistently outperformed the traditional SSI-cov method across all three states. The quantitative analysis shows that the SA-FCM algorithm improved accuracy by between 17.45% and 49.12% compared to the traditional SSI-cov method, especially in higher-order modes and more complex states. This substantial reduction in error demonstrates the effectiveness of the SA-FCM algorithm in identifying modal parameters more reliably and accurately, particularly in dynamic and constrained environments. The SA-FCM algorithm not only effectively handles the clustering of multiple modes but also optimizes the initialization process, thereby avoiding the local minimum issues often encountered with traditional methods. These improvements make SA-FCM a preferred algorithm for the modal identification of electric spindles.

An analysis of the experimental errors in the electric spindle revealed that they may have arisen from several factors: (1) The transient pulse excitation applied to the spindle system by the LC-1 impact hammer limited the energy input to the electric spindle system, potentially reducing the accuracy of experimental signals. (2) In simulation analysis, precise boundary conditions could not be fully replicated. Typically, the electric spindle casing was assumed to be fixed relative to the base, neglecting the stiffness of the connection. In addition, errors in the free state of the electric spindle were notably smaller than those in the constrained and dynamic states, which was attributable to the following: (1) Increased structural stiffness: Constraint application increased the overall system stiffness. (2) Boundary condition changes: The imposition of constraints restricted the spindle's motion, altering system boundary conditions [23,24]. The following are the causes of reduced errors in high-order modal frequencies: (1) In low-order modes, larger frequency disparities result from the dominance of overall motion characteristics (such as swinging or bending). These characteristics make low-order modes more vulnerable to changes in experimental setup, boundary conditions, and measurement errors. (2) In high-order modes, local vibration patterns are more prevalent. These patterns are less susceptible to measurement errors and experimental circumstances, leading to lesser inaccuracies [25–27].

The proposed automatic modal parameter identification method has significant practical implications for enhancing the dynamic performance and fault diagnosis capabilities of CNC machine tools. Integrating this method into real-time CNC control systems can significantly enhance the system's autonomous control capabilities. By continuously monitoring the spindle's modal parameters, the system can detect and mitigate abnormal dynamic behaviors in real time, thereby reducing the risk of machine failure, optimizing machining parameters, and improving product quality and production efficiency. Real-time feedback on modal parameters can further be used to adaptively adjust machining strategies, such as modifying cutting paths or feed rates, facilitating a more intelligent and responsive machining process.

7. Conclusions

Based on covariance-driven stochastic (SSI-cov) subspace methods combined with simulated annealing (SA) and fuzzy C-means clustering (FCM) algorithms, in this study, a novel method for identifying the modal parameters of electric spindles was proposed. Using finite element simulation models, the first five natural frequencies of electric spindles were extracted under different conditions, and these were validated using an experimental platform under ambient temperature conditions of 22 °C. The experimental data were subsequently processed using the proposed SSI-cov method combined with the SA-FCM algorithm to automatically extract the first five natural frequencies.

The comparison between simulation and experimental data demonstrated experiment errors of 0.17% to 0.33%, 1.05% to 3.27%, and 1.29% to 3.31% for the free, constrained, and dynamic states, respectively. Compared to the traditional SSI-cov method, the SA-FCM algorithm improved accuracy by 12.05% to 27.32% in the free state, 17.45% to 47.83% in the constrained state, and 25.45% to 49.12% in the dynamic state. The frequency identification

errors were controlled within the range of 2.25 Hz to 20.81 Hz, confirming the algorithm's ability to meet acceptable error tolerance standards. These results validate the algorithm's accuracy and reliability in identifying the modal parameters of electric spindles. The research results confirmed the feasibility and effectiveness of this algorithm in automatically extracting the modal parameters of electric spindles under different conditions, highlighting its significant practical implications for enhancing the dynamic performance and fault diagnosis capabilities of CNC machine tools.

Despite the algorithm's advantages, challenges remain in integrating it into practical CNC environments, particularly in optimizing real-time data processing and addressing noise and vibration issues. Future work should focus on improving computational efficiency and real-time adaptability and incorporating AI techniques to enhance robustness. Additionally, expanding the analysis to include mode shapes, damping characteristics, and uncertainty quantification will provide a more comprehensive understanding.

Author Contributions: Conceptualization, writing—review and editing, methodology, validation, W.Z.; writing—original draft preparation, formal analysis, data processing, L.Z. and W.K.; funding acquisition, project administration, supervision, resources, J.F., C.L. and Y.X. All authors have read and agreed to the published version of the manuscript.

Funding: This work is supported by the Zhejiang Provincial Natural Science Foundation (LDT23E0501, LDT23E05011E05), the National Natural Science Foundation of China (52175440), and the Key R&D Program of Zhejiang Province (2023C01058).

Data Availability Statement: Data are contained within this article.

Conflicts of Interest: The authors declare no conflicts of interest.

Nomenclature

t	Time
j	Maximum duration of output data
L	Toeplitz matrix
O	Observability matrix
Γ	Controllability matrix
$\sum_1$	Non-zero singular value part
U	Orthogonal matrices (left singular vector)
V	Orthogonal matrices (right singular vector)
S	Diagonal array of positive singular values
O_i	i-th order observability matrix
A_i	i-th system matrix
$(\bullet)^{\dagger}$	Pseudoinverse
A_c	Continuous-state space system matrix
A	Discrete-state space system matrix
Δt	Sampling time interval
μ_i	i-th eigenvalue matrix
λ	Eigenvalues in continuous-state space
μ	Eigenvalues in discrete-state space
f	Intrinsic frequency
ξ	Damping ratio
ϕ_i	i-th order modal matrix
C_i	i-th output matrix
ψ_i	i-th eigenvectors
n	System order
$E(t)$	Fitness of the current solution
T	Current temperature
$E(t+1)$	Fitness of the new solution
N	Number of initial clustering centers
N_m	Number of modal frequencies
q	Dimensions

V	Matrix of cluster center vectors
c	Cluster center vectors
v_i	i-th cluster center
μ_{ik}	Element of the matrix U
z_k	Membership degree of the k-th data point
J	Objective function
ε	Threshold
C	Number of cluster centers
m	Membership coefficient factor
$U^{(0)}$	Membership matrix
$V^{(t)}$	Cluster center vector
$U^{(t)}$	Membership matrix

References

1. Hsieh, M.C.; Maurya, S.N.; Luo, W.J.; Li, K.Y.; Hao, L.; Bhuyar, P. Coolant Volume Prediction for Spindle Cooler with Adaptive Neuro-fuzzy Inference System Control Method. *Sens. Mater.* **2022**, *34*, 2447–2466. [CrossRef]
2. Dai, Y.; Tao, X.; Li, Z.; Zhan, S.; Li, Y.; Gao, Y. A review of key technologies for high-speed motorized spindles of CNC machine tools. *Machines* **2022**, *10*, 145. [CrossRef]
3. Wang, L.; Zhao, Q.; Zhang, B. Accuracy of an electric spindle. *J. Tsinghua Univ. (Nat. Sci. Ed.)* **2018**, *58*, 746–751. [CrossRef]
4. Dai, Y.; Qiao, B.; Chen, X.; Pan, G. A review on high-speed electric spindle dynamics modeling and vibration response research. *Recent Pat. Eng.* **2023**, *19*, 1–27. [CrossRef]
5. Afshar, M.; Khodaygan, S. Enhanced stabilization diagram for automated modal parameter identification based on power spectral density transmissibility functions. *Struct. Control Health Monit.* **2019**, *26*, e2355. [CrossRef]
6. Colombo, F.; Lentini, L.; Trivella, A.; Raparelli, T.; Viktorov, V. Experimental and numerical dynamic identification of an aerostatic electro-spindle. *Appl. Sci.* **2021**, *11*, 11462. [CrossRef]
7. Sun, J.; Li, W.; Luo, C.; Yu, Q. Rotor Imbalance Recognition of Electric Spindle Based on Wavelet Packet and Random Forest. In Proceedings of the 2021 6th International Conference on Robotics and Automation Engineering (ICRAE), Guangzhou, China, 19–22 November 2021; pp. 212–216. [CrossRef]
8. Ubertini, F.; Gentile, C.; Materazzi, A.L. Automated modal identification in operational conditions and its application to bridges. *Eng. Struct.* **2013**, *46*, 264–278. [CrossRef]
9. Hong, A.L.; Ubertini, F.; Betti, R. Wind analysis of a suspension bridge: Identification and finite-element model simulation. *J. Struct. Eng.* **2011**, *137*, 133–142. [CrossRef]
10. Zhu, Q.; Wang, H.; Mao, J. Automated modal parameter identification method for bridges based on cluster analysis. *J. Southeast Univ. (Nat. Sci. Ed.)* **2020**, *50*, 837–843. [CrossRef]
11. Huang, Y.; Chen, T.; Zhu, B. Modal features real-time extraction of offshore platform based on stochastic subspace method. *J. Vib. Shock* **2021**, *40*, 147–155. [CrossRef]
12. Liu, W.; Yang, N.; Bai, F.; Chang, P. Parameter optimization of covariance-driven stochastic subspace identification method based on sensitivity analysis. *Eng. Mech.* **2021**, *38*, 157–167+178. [CrossRef]
13. Reynders, E. Uncertainty quantification in data-driven stochastic subspace identification. *Mech. Syst. Signal Process.* **2021**, *151*, 107338. [CrossRef]
14. Maurya, S.N.; Li, K.Y.; Luo, W.J.; Kao, S.Y. Effect of coolant temperature on the thermal compensation of a machine tool. *Machines* **2022**, *10*, 1201. [CrossRef]
15. Maurya, S.N.; Luo, W.J.; Panigrahi, B.; Negi, P.; Wang, P.T. Input attribute optimization for thermal deformation of machine-tool spindles using artificial intelligence. *J. Intell. Manuf.* **2024**, 1–22. [CrossRef]
16. Su, L.; Song, M.; Dong, S.; Luo, Y. Automatic analysis of stabilization diagram using iterative genetic-fuzzy clustering method. *J. Zhejiang Univ. (Eng. Sci.)* **2017**, *51*, 514–523. [CrossRef]
17. Liu, Y.; Glass, G. Effects of mesh density on finite element analysis. In Proceedings of the SAE 2013 World Congress & Exhibition, Detroit, MI, USA, 16–18 April 2013. [CrossRef]
18. Li, Y.; Chen, X.; Zhang, P.; Zhou, J. Dynamics modeling and modal experimental study of high speed motorized spindle. *J. Mech. Sci. Technol.* **2017**, *31*, 1049–1056. [CrossRef]
19. Wagg, D.; Neild, S. *Modal Analysis for Structural Dynamics: Modeling, Testing and Applications*, 1st ed.; Springer: Berlin/Heidelberg, Germany, 2015.
20. O'Connell, B.J.; Rogers, T.J. A robust probabilistic approach to stochastic subspace identification. *J. Sound Vib.* **2024**, *581*, 118381. [CrossRef]
21. Reynders, E.; De Roeck, G. Reference-based combined deterministic-stochastic subspace identification for experimental and operational modal analysis. *Mech. Syst. Signal Process.* **2008**, *22*, 617–637. [CrossRef]
22. Pastor, M.; Binda, M.; Harčarik, T. Modal assurance criterion. *Procedia Eng.* **2012**, *48*, 543–548. [CrossRef]
23. Ewins, D.J. *Modal Testing: Theory, Practice, and Application*, 1st ed.; Research Studies Press Ltd.: Baldock, UK, 2000.
24. Craig, R.R.; Kurdila, A.J. *Fundamentals of Structural Dynamics*, 2nd ed.; John Wiley & Sons: Hoboken, NJ, USA, 2006.

25. Wixom, A.; McDaniel, J. High order modal approximation techniques in the frequency domain. *J. Acoust. Soc. Am.* **2015**, *137*, 2342. [CrossRef]
26. Ege, K.; Boutillon, X.; David, B. High-resolution modal analysis. *J. Sound Vib.* **2009**, *325*, 852–869. [CrossRef]
27. Imai, J. Modeling uncertainty of flexible structures with unknown high-order modal parameters—A geometric characterization of frequency responses. In Proceedings of the 41st SICE Annual Conference, SICE 2002, Osaka, Japan, 5–7 August 2002; Volume 3, pp. 1588–1591. [CrossRef]

Disclaimer/Publisher's Note: The statements, opinions and data contained in all publications are solely those of the individual author(s) and contributor(s) and not of MDPI and/or the editor(s). MDPI and/or the editor(s) disclaim responsibility for any injury to people or property resulting from any ideas, methods, instructions or products referred to in the content.